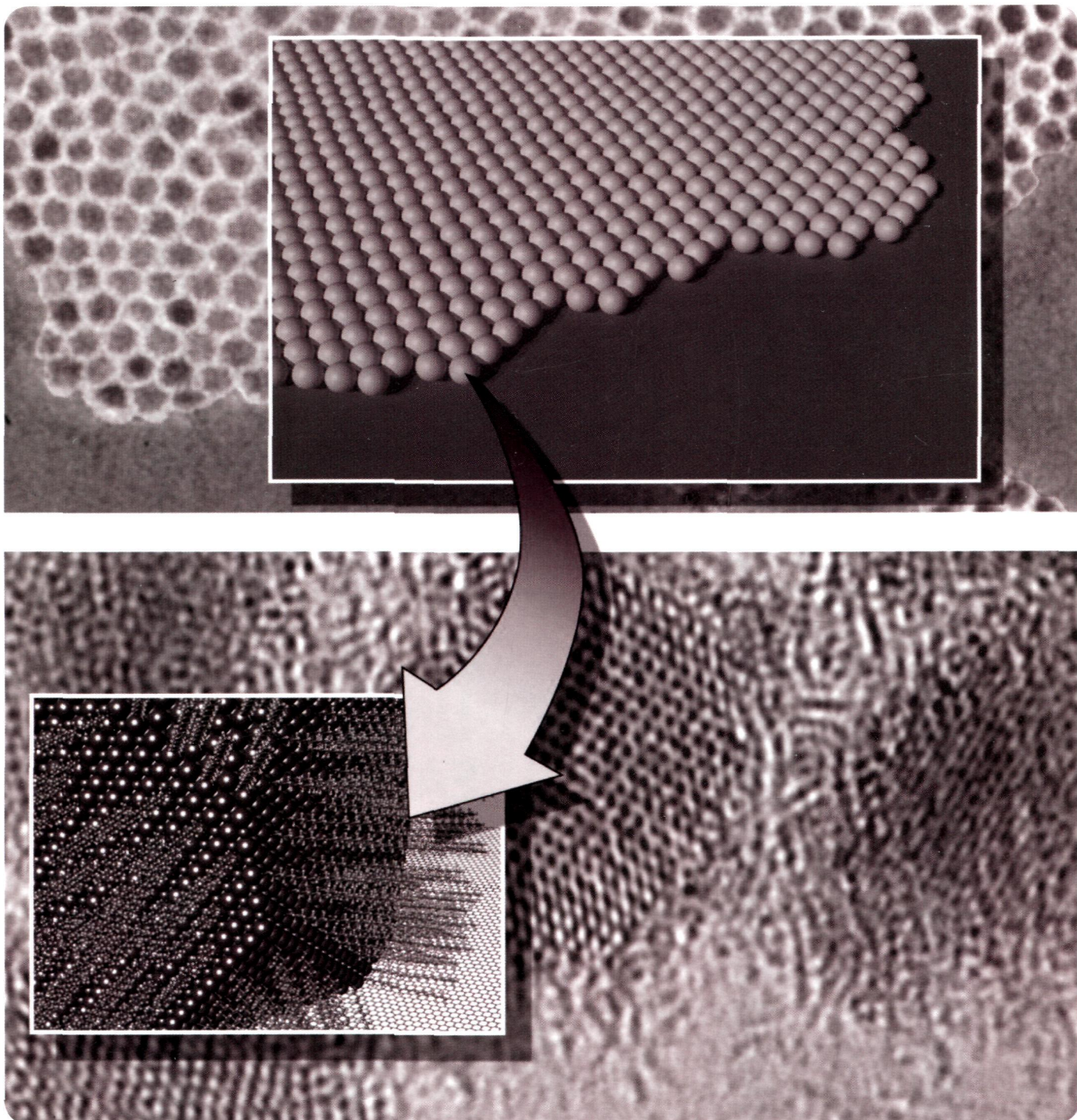


cm CHEMISTRY OF MATERIALS

FEBRUARY 25, 2014 | VOLUME 26 | NUMBER 4 | pubs.acs.org/cm



ACS Publications

MOST TRUSTED. MOST CITED. MOST READ.

www.acs.org

ON THE COVER: Lead telluride nanocrystals self-assembled into a close-packed monolayer when deposited onto graphene. This permitted their high resolution characterization by aberration corrected transmission electron microscopy. For more information, see "PbTe Nanocrystal Arrays on Graphene and the Structural Influence of Capping Ligands" by Alex W. Robertson, Camden Ford, Kuang He, Angus I. Kirkland, Andrew A. R. Watt, and Jamie H. Warner* (*Chem. Mater.* 2014, 26, 1567–1575).

Editorial

1501

dx.doi.org/10.1021/cm500494z

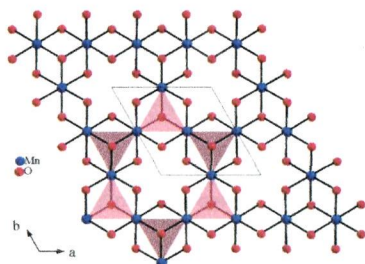
Chemistry and Materials in the Spotlight at the Dallas Spring Meeting

Jillian M. Buriak

Communications

1502

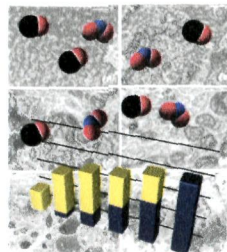
S

dx.doi.org/10.1021/cm403237u**KMn₃O₂(Ge₂O₇): An S = 2 Magnetic Insulator Featuring Pillared Kagome Lattice**
Matthew S. Williams, J. Palmer West, and Shiou-Jyh Hwu*

1505

Chemical Tuning versus Microstructure Features in Solid-State Gas Sensors: $\text{LaFe}_{1-x}\text{Ga}_x\text{O}_3$, a Case Study

Marta Maria Natile,* Andrea Ponzoni, Isabella Concina, and Antonella Glisenti

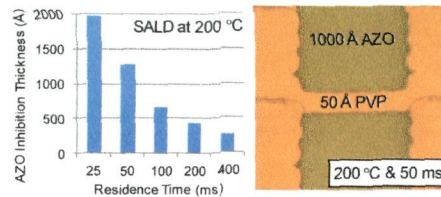


dx.doi.org/10.1021/cm4018858

1514

Selective Area Spatial Atomic Layer Deposition of ZnO , Al_2O_3 , and Aluminum-Doped ZnO Using Poly(vinyl pyrrolidone)

Carolyn R. Ellinger* and Shelby F. Nelson



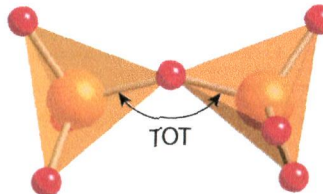
dx.doi.org/10.1021/cm402464z

1523



Ab Initio Calculations of the Energy Dependence of Si–O–Si Angles in Silica and Ge–O–Ge Angles in Germania Crystalline Systems

Colby J. Dawson, Rebeca Sanchez-Smith, Peter Rez, Michael O'Keeffe, and Michael M. J. Treacy*



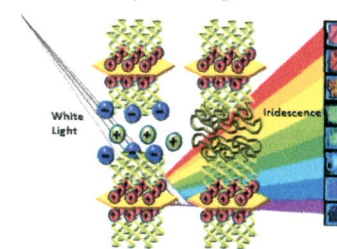
dx.doi.org/10.1021/cm402814v

1528



Solution Processable Iridescent Self-Assembled Nanoplatelets with Finely Tunable Interlayer Distances Using Charge- and Sterically Stabilizing Oligomeric Polyoxalkyleneamine Surfactants

Minhao Wong, Ryohei Ishige, Taiki Hoshino, Spencer Hawkins, Peng Li, Atsushi Takahara, and Hung-Jue Sue*

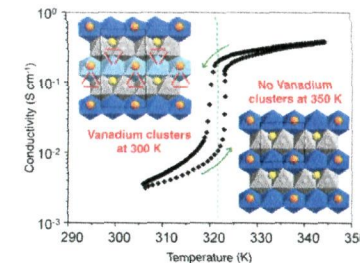


dx.doi.org/10.1021/cm403114k

1538

Vanadium Clustering/Declustering in $\text{P}_2\text{–Na}_{1/2}\text{VO}_2$ Layered Oxide

Marie Guignard,* Dany Carlier, Christophe Didier, Matthew R. Suchomel, Erik Elkaïm, Pierre Bordet, Rodolphe Decourt, Jacques Darriet, and Claude Delmas

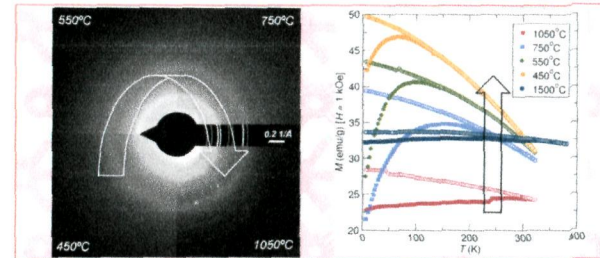


dx.doi.org/10.1021/cm403167a

1549

Size and Crystallinity Dependence of Magnetism in Nanoscale Iron Boride, $\alpha\text{-FeB}$

Steffi Rades, Stephan Kraemer, Ram Seshadri,* and Barbara Albert*



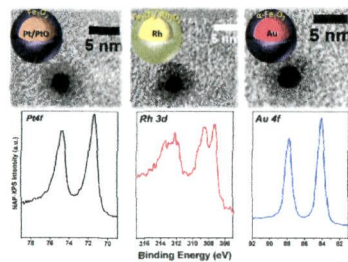
7A

Chemistry of Materials, Volume 26, Issue 4

6A

Chemistry of Materials, Volume 26, Issue 4

Mixing Patterns and Redox Properties of Iron-Based Alloy Nanoparticles under Oxidation and Reduction Conditions
 Vasiliki Papaefthimiou, Florent Tournus, Arnaud Hillion, Ghassan Khadra, Detre Teschner, Axel Knop-Gericke, Veronique Dupuis, and Spyridon Zafeiratos*



dx.doi.org/10.1021/cm403172a

Chemical Control of Thermal Expansion in Cation-Exchanged Zeolite A

Thomas Carey, Chiu C. Tang, Joseph A. Hriljac,* and Paul A. Anderson*

Figure 8B illustrates the chemical control of thermal expansion in cation-exchanged zeolite A. It shows three structures: ITQ-29 (top left), Dehydrated Ag-A (middle left), and Dehydrated Na-A (right). The structures are shown with their respective pore sizes indicated: 2.9 Å for ITQ-29, 2.3 Å for Dehydrated Ag-A, and 2.4 Å for Dehydrated Na-A. Arrows indicate the movement of framework atoms upon dehydration.

dx.doi.org/10.1021/cm403312q

1567

S

PbTe Nanocrystal Arrays on Graphene and the Structural Influence of Capping Ligands

Alex W. Robertson, Camden Ford, Kuang He, Angus I. Kirkland, Andrew A. R. Watt, and Jamie H. Warner*

Figure 8C shows the synthesis of PbTe nanocrystals. It starts with PbTe dissolved in EtOH, followed by addition of a mixture of EtOH, H₂O, and Graphene. This leads to 'Ligand exchange' and 'Crosslinked aggregation' of the nanocrystals. The final product is a 'Crosslinked aggregation' of PbTe nanocrystals on a graphene substrate.

dx.doi.org/10.1021/cm403373q

1576

S

Controlling the Structural and Optical Properties of Ta₃N₅ Films through Nitridation Temperature and the Nature of the Ta Metal
 Blaise A. Pinaud, Arturas Vailionis, and Thomas F. Jaramillo*

dx.doi.org/10.1021/cm403482s

Figure 9A illustrates the growth of Ta₃N₅ films. On the left, 'Structural information' shows a cross-section of the film layers: Ta₃N₅, Ta₂N, Ta, and fused silica. An inset shows a TEM image of the film. On the right, 'Optical information' shows a color gradient from 'Thin' (blue) to 'Thick' (red) Ta₃N₅ films, with a schematic showing light scattering from the surface.

1583

Influence of the Kinetic Adsorption Process on the Atomic Layer Deposition Process of (GeTe)_(1-x)(Sb₂Te₃)_x Layers Using Ge⁴⁺-Alkoxide Precursors

Taeyong Eom, Taehong Gwon, Sijung Yoo, Byung Joon Choi, Moo-Sung Kim, Iain Buchanan, Manchao Xiao, and Cheol Seong Hwang*

Figure 9B is a plot of 'Growth rate (nm cm⁻² s⁻¹)' versus 'Substrate temperature (°C)'. The y-axis ranges from 0 to 140, and the x-axis ranges from 40 to 120. Two data series are shown: 'Exp. Theo.' (black squares) and 'Ge(OCH₃)₄' (red circles). Both series show a decreasing trend as the substrate temperature increases, with the theoretical values being higher than the experimental values.

dx.doi.org/10.1021/cm4034885

1592

dx.doi.org/10.1021/cm403505s

Nanophotosensitizers Engineered to Generate a Tunable Mix of Reactive Oxygen Species, for Optimizing Photodynamic Therapy, Using a Microfluidic Device

Hyung Ki Yoon, Xia Lou, Yu-Chih Chen, Yong-Eun Koo Lee, Euisik Yoon, and Raoul Kopelman*

Figure 9C shows a microfluidic setup for generating reactive oxygen species. It consists of a microfluidic channel where MB-PEGDMA and PAAs NPs are mixed. The mixture is then exposed to light from an LED. The resulting ROS generation is measured using a fluorescence microscope and quantified in a bar chart.

8A

Chemistry of Materials, Volume 26, Issue 4

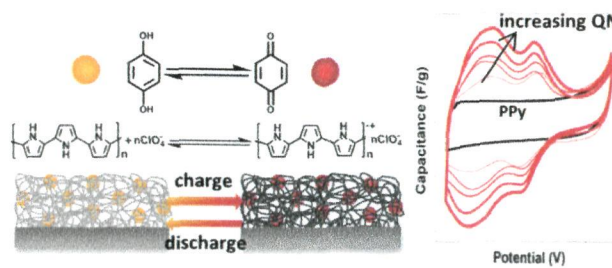
9A

Chemistry of Materials, Volume 26, Issue 4

Redox Solute Doped Polypyrrole for High-Charge Capacity Polymer Electrodes

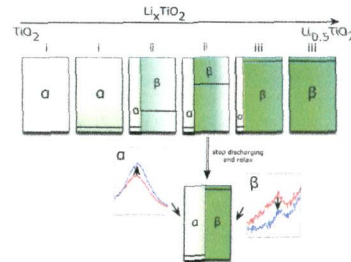
Margarita R. Arcila-Velez and Mark E. Roberts*

dx.doi.org/10.1021/cm403630h

**Impact of Particle Size on the Non-Equilibrium Phase Transition of Lithium-Inserted Anatase TiO₂**

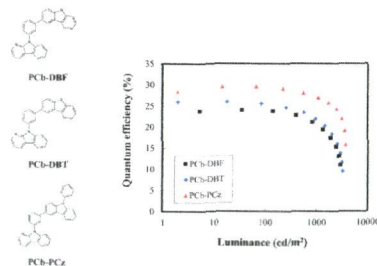
Kun Shen, Hao Chen, Frits Klaver, Fokko M. Mulder, and Marnix Wagemaker*

dx.doi.org/10.1021/cm4037346

**Structure–Property Relationship of Pyridoindole-Type Host Materials for High-Efficiency Blue Phosphorescent Organic Light-Emitting Diodes**

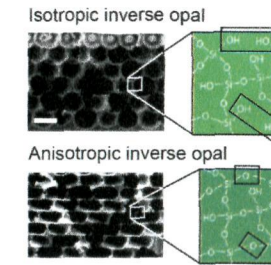
Chil Won Lee and Jun Yeob Lee*

dx.doi.org/10.1021/cm403750p

**Tunable Anisotropy in Inverse Opals and Emerging Optical Properties**

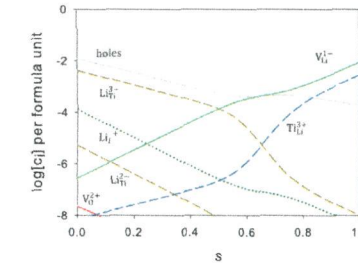
Katherine R. Phillips, Nicolas Vogel, Yuhang Hu, Mathias Kolle, Carole C. Perry, and Joanna Aizenberg*

dx.doi.org/10.1021/cm403812y

**Point Defects and Non-stoichiometry in Li₂TiO₃**

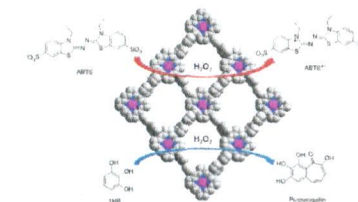
Samuel T. Murphy* and Nicholas D. M. Hine

dx.doi.org/10.1021/cm4038473

**Covalent Heme Framework as a Highly Active Heterogeneous Biomimetic Oxidation Catalyst**

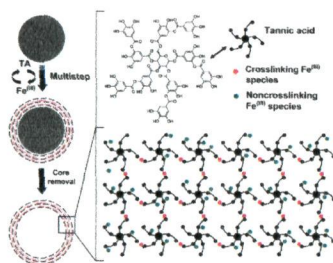
Xi-Sen Wang, Matthew Chrzanowski, Daqiang Yuan, Brandon S. Sweeting, and Shengqian Ma*

dx.doi.org/10.1021/cm403860t



Coordination-Driven Multistep Assembly of Metal-Polyphenol Films and Capsules

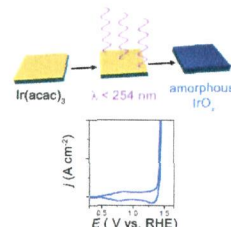
Md. Arifur Rahim, Hirotaka Ejima, Kwun Lun Cho, Kristian Kempe, Markus Müllner, James P. Best, and Frank Caruso*



dx.doi.org/10.1021/cm403903m

Facile Photochemical Preparation of Amorphous Iridium Oxide Films for Water Oxidation Catalysis

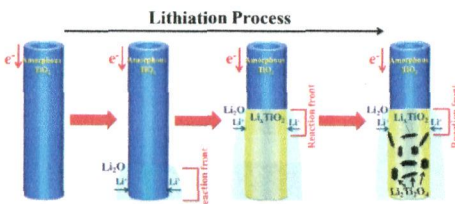
Rodney D. L. Smith, Barbora Sporinova, Randal D. Fagan, Simon Trudel,* and Curtis P. Berlinguette*



dx.doi.org/10.1021/cm4041715

Direct Evidence of Lithium-Induced Atomic Ordering in Amorphous TiO_2 Nanotubes

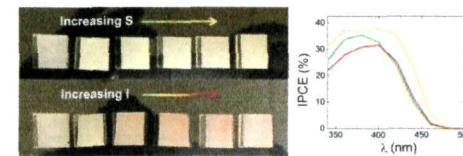
Qi Gao, Meng Gu, Anmin Nie, Farzad Mashayek, Chongmin Wang,* Gregory M. Odegard, and Reza Shahbazian-Yassar*



dx.doi.org/10.1021/cm403951b

Improved Visible Light Harvesting of WO_3 by Incorporation of Sulfur or Iodine: A Tale of Two Impurities

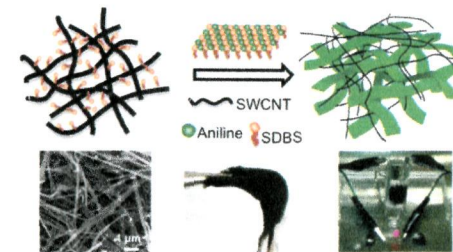
Alexander J. E. Rettie, Kyle C. Klavetter, Jung-Fu Lin, Andrei Dolocan, Hugo Celio, Ashoma Ishiekwene, Heather L. Bolton, Kristen N. Pearson, Nathan T. Hahn, and C. Buddie Mullins*



dx.doi.org/10.1021/cm403969r

In Situ Synthesis of Hybrid Aerogels from Single-Walled Carbon Nanotubes and Polyaniline Nanoribbons as Free-Standing, Flexible Energy Storage Electrodes

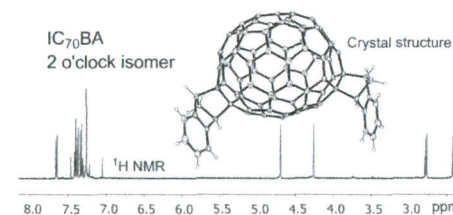
Dengteng Ge, Lili Yang,* Apiradee Honglawan, Jie Li, and Shu Yang*



dx.doi.org/10.1021/cm404025g

Single Isomer of Indene-C₇₀ Bisadduct—Isolation and Performance in Bulk Heterojunction Solar Cells

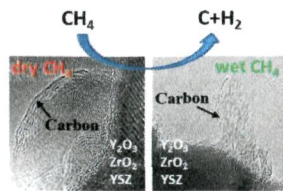
Wallace W. H. Wong,* Jegadesan Subbiah, Jonathan M. White, Helga Seyler, Bolong Zhang, David J. Jones, and Andrew B. Holmes



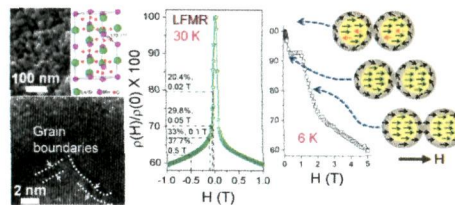
dx.doi.org/10.1021/cm404054z

Methane Decomposition and Carbon Growth on Y_2O_3 , Yttria-Stabilized Zirconia, and ZrO_2 Author: ACS style guidelines allow only certain abbreviations in the title. To comply with the guidelines, YSZ has been spelled out.

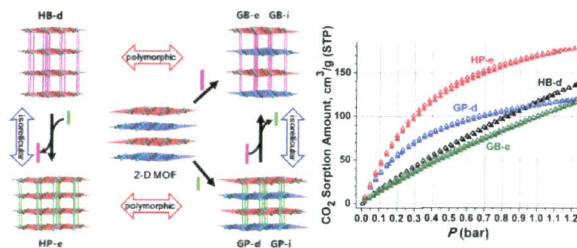
Michaela Kogler, Eva-Maria Köck, Lukas Perfler, Thomas Bielz, Michael Stöger-Pollach, Walid Hetaba, Marc Willinger, Xing Huang, Manfred Schuster, Bernhard Klötzer, and Simon Penner*



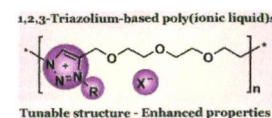
Enhanced Low-Field Magnetoresistance in $\text{La}_{0.71}\text{Sr}_{0.29}\text{MnO}_3$ Nanoparticles Synthesized by the Nonaqueous Sol–Gel Route
Anustup Sadhu and Sayan Bhattacharyya*



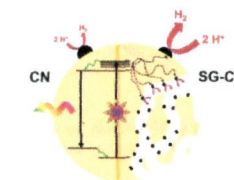
Combinational Synthetic Approaches for Isoreticular and Polymorphic Metal–Organic Frameworks with Tuned Pore Geometries and Surface Properties
Seok Jeong, Dongwook Kim, Sunyoung Shin, Dohyun Moon, Sung June Cho, and Myoung Soo Lah*



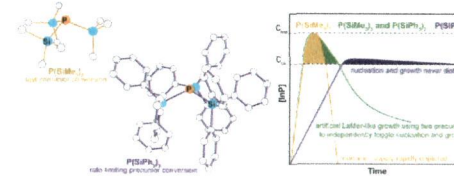
1,2,3-Triazolium-Based Poly(ionic liquid)s with Enhanced Ion Conducting Properties Obtained through a Click Chemistry Polyaddition Strategy
Bhanu P. Mudraboyna, Mona M. Obadia, Imène Allaoua, Rakhi Sood, Anatoli Serghei, and Eric Drockenmuller*



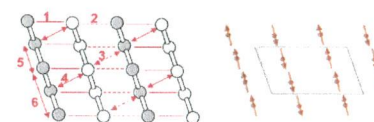
Structure–Activity Relationships in Bulk Polymeric and Sol–Gel-Derived Carbon Nitrides during Photocatalytic Hydrogen Production
Dirk Hollmann,* Michael Karnahl, Stefanie Tschierlei, Kamalakannan Kailasam, Matthias Schneider, Jörg Radnik, Kathleen Grabow, Ursula Bentrup, Henrik Junge, Matthias Beller, Stefan Lochbrunner, Arne Thomas,* and Angelika Brückner*



Investigation of Indium Phosphide Quantum Dot Nucleation and Growth Utilizing Triarylsilylphosphine Precursors
Dylan C. Gary, Benjamin A. Glassy, and Brandi M. Cossairt*

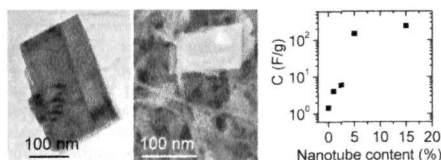


Analysis of the Difference between the Pyroxenes $\text{LiFeSi}_2\text{O}_6$ and $\text{LiFeGe}_2\text{O}_6$ in Their Spin Order, Spin Orientation, and Ferrotoroidal Order
Changhoon Lee, Jinhee Kang, Jisook Hong, Ji Hoon Shim,* and Myung-Hwan Whangbo*



Production of Molybdenum Trioxide Nanosheets by Liquid Exfoliation and Their Application in High-Performance Supercapacitors

Damien Hanlon, Claudia Backes, Thomas M. Higgins, Marguerite Hughes, Arlene O'Neill, Paul King, Niall McEvoy, Georg S. Duesberg, Beatriz Mendoza Sanchez, Henrik Pettersson, Valeria Nicolosi, and Jonathan N. Coleman*

**Additions and Corrections****Correction to Synthesis, Exfoliation, and Electronic/Protonic Conductivity of the Dion–Jacobson Phase Layer Perovskite $\text{HLa}_2\text{Ti}_2\text{TaO}_{10}$**

TsingHai Wang, Camden N. Henderson, Thomas I. Draskovic, and Thomas E. Mallouk*